doi:10.26443/seismica.v4i1.1214

Evidence for Far-Field Wastewater Disposal Causing Recent Increases in Seismicity in Central and Northern Kansas

S. L. Fasola *[1,2], **M. R. Brudzinski** [3], **N. M. Jackson** [1]

[1]Department of Geology, University of Kansas, Lawrence, KS, United States, [2]Now at the Cascadia Region Earthquake Science Center, Eugene, OR, United States, [3]Department of Geology and Environmental Earth Science, Miami University, Oxford, OH, United States

Author contributions: *Conceptualization*: S.L.F., M.R.B., N.M.J.. *Data Curation*: S.L.F.. *Formal Analysis*: S.L.F., M.R.B.. *Funding Acquisition*: N.M.J.. *Investigation*: S.L.F.. *Methodology*: S.L.F., M.R.B.. *Resources*: N.M.J.. *Software*: S.L.F., M.R.B.. *Supervision*: N.M.J.. *Visualization*: S.L.F., N.M.J.. *Writing – original draft*: S.L.F.. *Writing – review & editing*: S.L.F., M.R.B., N.M.J..

Abstract The rate of felt earthquakes in Kansas increased dramatically in 2014, where most seismicity initially occurred in southern Kansas, and was attributed to large-volume wastewater disposal (WD) near the Oklahoma-Kansas border. Interestingly, 9 of 10 magnitude 4+ earthquakes from 2019-2022 occurred in northern and central Kansas, where the nature of seismicity has not been explored. We investigated seismicity near the recent M4+ earthquakes using waveform cross-correlation and carefully assembled injection and extraction volumes, well stimulations, and pressure measurements. Waveform cross-correlation reveals earthquakes occur via swarms with low b-values implying a stress state that is closer to failure. Relative volumes and temporal trends indicate seismicity was primarily induced by WD into the Arbuckle. However, the large coefficient of variation of interevent times suggests primarily far-field pressure influences. In particular, Jewell County seismicity provides strong evidence of far-field forcing as it occurs >50 km from any WD wells and ∼100 km from large volume WD wells, one of the largest distances of WD-induced seismicity documented. The heterogenous locations of seismicity relative to WD wells is likely controlled by preexisting unknown structures and prestresses. These results imply a large spatial influence from proposed large volume carbon sequestration in the Arbuckle and similar formations.

Production Editor: Gareth Funning
Handling Editor: Yen Joe Tan
Copy & Layout Editor: Théa Ragon

Received: February 9, 2024
Accepted: April 10, 2025
Published: May 7, 2025

1 Introduction

The largest known induced earthquakes have been linked to wastewater disposal (WD) in Oklahoma where copious amounts of fluids have been injected into the Cambrian-Ordovician Arbuckle Group (hereinafter the Arbuckle). Large earthquakes include the 2016 M_W 5.8 Pawnee (Yeck et al., 2017) and 2011 M_W 5.7 Prague (Keranen et al., 2013) earthquakes. The potential for these larger magnitude events to cause damage underscores the need to understand the causes of injection induced seismicity. The generally accepted model for injection induced seismicity is that one to a few wells injecting at high rates locally increases pore fluid pressures reducing the effective normal stress on pre-existing, critically stressed faults in the crystalline basement facilitating seismicity (Ellsworth, 2013). There are clear cases of far-field triggering, up to 40 km, as well (Keranen et al., 2014; Yeck et al., 2016; Haddad and Eichhubl, 2022) indicating that faults which become seismically active have various thresholds for how much pore pressure change is required for the fault to reach criticality.

The issue of induced seismicity spread to southern Kansas where, as in Oklahoma, large amounts of fluids have been injected into the subsurface over the last few decades. Fluids are injected through Class I and Class II wells. Class I wells, regulated by the Kansas Department of Health and Environment (KDHE), dispose of hazardous and nonhazardous industrial and municipal fluids. All but one of the 50 Class I wells in Kansas are injecting into the Arbuckle. Class II wells, regulated by the Kansas Corporation Commission (KCC), consist of saltwater disposal (SWD) and enhanced oil recovery (EOR) wells. SWD wells permanently dispose of formation brines coproduced during oil and gas production while EOR wells inject fluids (typically recycled water from production and/or CO_2) to mobilize oil and/or gas into production wells. The majority of SWD wells inject into the Arbuckle which typically overlies the Precambrian crystalline basement (Franseen et al., 2004) while EOR wells are mainly targeting shallower intervals. On the Central Kansas Uplift (CKU), the uppermost Arbuckle has also been a primary producing reservoir up until the development of unconventional drilling (i.e., hydraulic fracturing [HF]) of the Mississippi Lime Play in southern Kansas (Franseen et al., 2004). Due to the renewed interest in the water-rich Mississippi Lime Play in 2011, production and subsequently disposal rose in Kansas.

Historically, Kansas is generally a seismically quiet state, with an average of three M≥2 earthquakes per year and one M≥3 earthquake every two years, most of which occurred on the CKU and near the Nemaha Ridge-Humboldt fault system (Supplemental Figure

*Corresponding author: sfasola@uoregon.edu

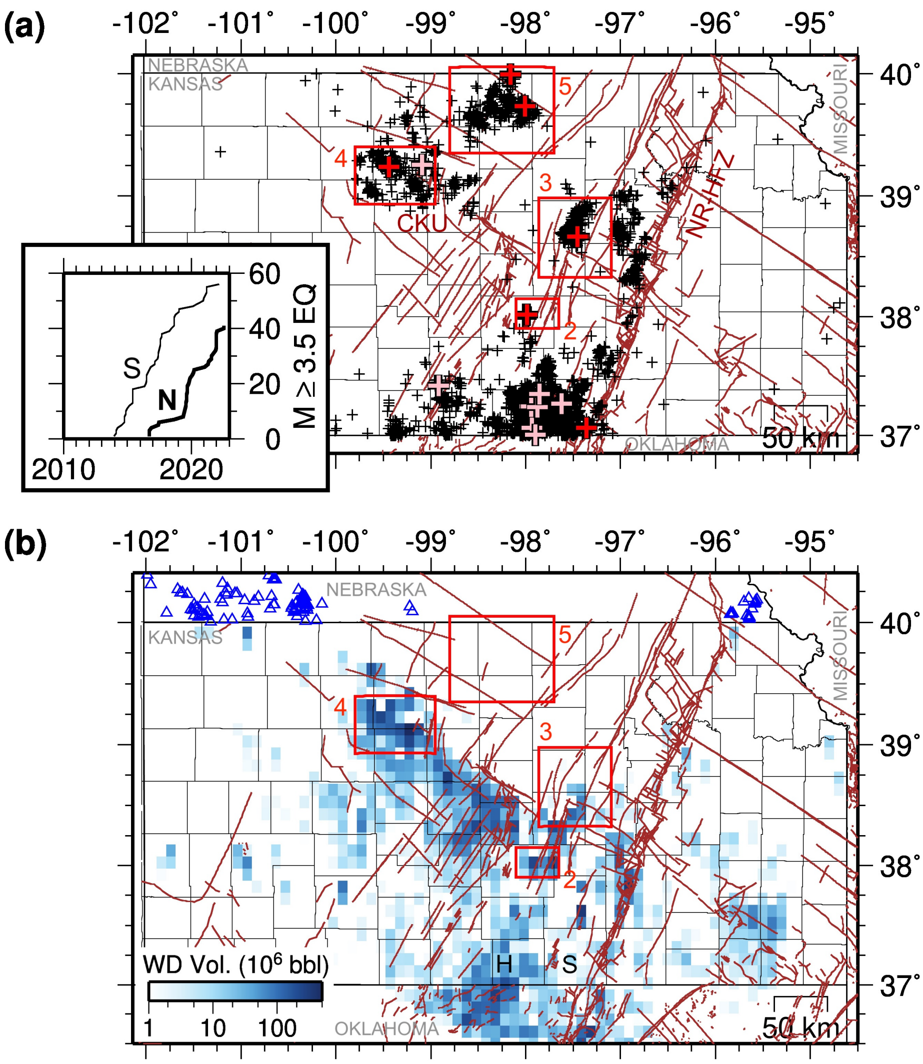

Figure 1 (a) Map of 2000-2022 KGS and ComCat earthquakes (black crosses; M≥4 colored pink if before 2019 and red if after 2019). Faults (brown; Mohammadi et al., 2022) and counties (black) are outlined. Red boxes mark the four focus regions in this study corresponding to Figures 2-5. Major geologic structures are abbreviated as CKU, Central Kansas Uplift; NR-HFZ, Nemaha Ridge-Humboldt Fault Zone. Inset shows cumulative number of M≥3.5 earthquakes for north (thick line) and south (thin line) of 37.75°. (b) Map of total injected volume (2000-2022) from Arbuckle WD wells computed in 0.1°×0.1° bins. Harper [H] and Sumner [S] counties are labeled. Blue triangles represent locations of WD wells from all intervals in Nebraska as volumes were not available.

S1a). However, the number of M≥3 earthquakes dramatically increased in 2014, such that the average grew to 42 times the background rate, the second highest seismicity rate increase in the central United States at that time (Rubinstein et al., 2018). The increase in seismicity was primarily observed in south-central Kansas with 83% of southern seismicity in Harper and Sumner counties near the Oklahoma border. Several studies attributed this rise of seismicity to the concurrent rise in WD where seismicity was primarily driven by the rate of pressure increases induced from wells injecting into the Arbuckle in southern Kansas and northern Oklahoma (Langenbruch et al., 2018; Peterie et al., 2018; Rubinstein et al., 2018; Schoenball and Ellsworth, 2017a). Zhai et al. (2020) found that injection in Oklahoma amplified the total Coulomb stress change (1.5x) and seismicity rate (3x) in south-central Kansas. Most of the earthquakes occurred in the crystalline basement at a mean depth of 6.5 km, suggesting increased pore fluid pressures within the Arbuckle increased the potential for slip on hydraulically connected basement faults (Rubinstein et al., 2018; Schoenball and Ellsworth, 2017a). The largest recorded earthquake in Kansas was the injection-induced 2014 M_W 4.9 Milan earthquake in Sumner County, whose felt reports included cracked plaster, items thrown from shelves, and structural damage to some buildings constructed of unreinforced masonry (Choy et al., 2016; Hearn et al., 2018).

In response to the elevated seismic hazard in south-central Kansas, the state government of Kansas formed a task force composed of the KCC, KDHE, and Kansas Geological Survey (KGS) which developed and implemented a seismic action plan that included increased seismic monitoring and a staged reduction of wastewater injection for south-central Kansas (Buchanan et al., 2023). The rate of seismicity soon dropped in south-central Kansas following implementation of regulations in 2015 and 2016 but by mid-2017 earthquakes had migrated north into Sedgwick and Reno (city of Hutchinson) counties as much as 90 km from initial swarm locations (Peterie et al., 2018). Peterie et al. (2018) concluded that the Hutchinson swarm was influenced by fluid diffusion from high-volume injection wells near the Kansas-Oklahoma border nearly 90 km away, much farther than what has been previously observed in cases of far-field pore pressure diffusion (∼40 km; Keranen et al., 2014; Yeck et al., 2016; Haddad and Eichhubl, 2022).

While two-thirds of Kansas seismicity since 2014 has been in south-central Kansas and attributed to WD into the Arbuckle, this study seeks to investigate the causes of the less studied seismicity in northern and central Kansas (Figure 1). There have been ten M≥4 earthquakes in Kansas from 2019-2022, including two M 4.8 events. Interestingly, nine of those ten occurred north of the well-documented seismicity in Harper and Sumner counties, and besides the work done by Peterie et al. (2018) on the Hutchinson earthquakes, there has been a lack of investigation into the causes of northern and central Kansas seismicity. Therefore, this study investigates potential causes of increased seismicity in northern and central Kansas by integrating multiple datasets and performing template matching to enhance earthquake detections. We focus on regions with M≥4 earthquakes: Hutchinson, Salina, northern region of the CKU, and Jewell County (Figure 1). Furthermore, the Arbuckle has been proposed as a target for geologic storage of CO_2 (Schwab et al., 2017), highlighting the importance for understanding the nature of seismicity in the state.

Enhancing detection of seismicity has been an effective strategy for discerning the causes of anomalous increased seismicity rates potentially associated with fluid injection (e.g., Schultz et al., 2020). More detailed temporal patterns of seismicity provide additional information to the spatial and temporal correlation of operational activities and seismicity which has been the primary criteria for determining whether seismicity was human induced (Davis and Frohlich, 1993). It has been particularly helpful to identify whether the seismicity has swarm-like characteristics (Skoumal et al., 2015): the largest event is not at the beginning, multiple events near the maximum magnitude, lack of Omori decay. Increased fluid pressure is commonly cited as the cause of earthquake swarms in natural settings (e.g., Vidale and Shearer, 2006). Thus, this study will use swarm-like characteristics along with the spatial and temporal associations of seismicity with operational activities and subsurface pressures to interpret the recent increases in Kansas seismicity

2 Methods

To enhance the detection of seismicity in the regions surrounding the M≥4 earthquakes, we pursued waveform cross-correlation ("template matching") using earthquakes from the KGS and Advanced National Seismic System (ANSS) comprehensive catalog (ComCat) as templates. We utilized the cross-correlation detector in the ObsPy Python package (Beyreuther et al., 2010) to scan continuous three-component waveform data from a single station (see Supplemental Material for further details). Matched events were confirmed with manual inspection (Supplemental Figure S2). Magnitudes of the matched events were estimated as in Schaff and Richards (2014). The nearest long-standing stations used for template matching were 1) N4 R32B from 2014-2022 for Hutchinson templates, 2) US KSU1 from 2010-2022 for Salina templates, 3) US CBKS from 2010-2022 for CKU and Jewell templates (Supplemental Figure S1b). Stations GS KS28 and KS JLK were also used for template matching in Hutchinson from August 2019 to December 2022 and Jewell County region from July 2017 to July 2022, respectively, as these newer stations were closer to seismicity. Template matched events from all four regions are available in the Supplemental Material (Dataset S1). The magnitude of completeness (M_C) was determined using the maximum curvature algorithm (Wiemer, 2000).

B-values are notoriously unstable and difficult to calculate, especially over long time scales with variable M_C. Thus, we calculated b-values with van der Elst (2021)'s new method which does not require the estimation of M_C: the b-positive method (Supplemental Figure S3). The b-positive method is based on magnitude differences between consecutive earthquakes, instead of relying on earthquake magnitudes as in the traditional Gutenberg-Richter b-value estimation of Bender (1983). The b-positive (b^+) method is as follows:

$$b^+ = 1/[\ln_{10}(\mathrm{M}'_{\mathrm{avg}} - \mathrm{M}'_{\mathrm{min}})] \quad (1)$$

where M'_{avg} is the average magnitude difference and M'_{min} is the minimum magnitude difference. We calculated the b-positive value for earthquakes within the four regions, the December 2021 Salina swarm, and the May-December 2019 CKU swarm.

The temporal pattern of seismicity was evaluated in each of the four study regions by calculating the coefficient of variation (CoV) of the time between earthquakes (e.g., Kagan and Jackson, 1991). The CoV has been defined as the ratio of the standard deviation of interevent times to the average interevent time of the earthquakes (Kagan and Jackson, 1991). We performed this calculation on geographical bins of approximately 1 degree in size with at least 100 events using the catalog resulting from template matching (Skoumal et al., 2019). If earthquakes are randomly distributed in time, we would expect CoV ≈ 1, while CoV < 1 represents periodic seismicity and CoV > 1 indicates temporal clustering (Kagan and Jackson, 1991; Cochran et al., 2018).

Our investigation into the nature of seismicity incorporated data from Class I, Class II, HF, and production wells (see Data and Resources). Data for Class I wells included monthly and annual injection volumes (Dataset S2) and formation pressures (Dataset S3), which were approximated through Horner analysis during required annual pressure falloff tests (Ansari et al., 2019). Following the approach in Ansari et al. (2019), we used locally weighted regression to fit a smoothing curve to

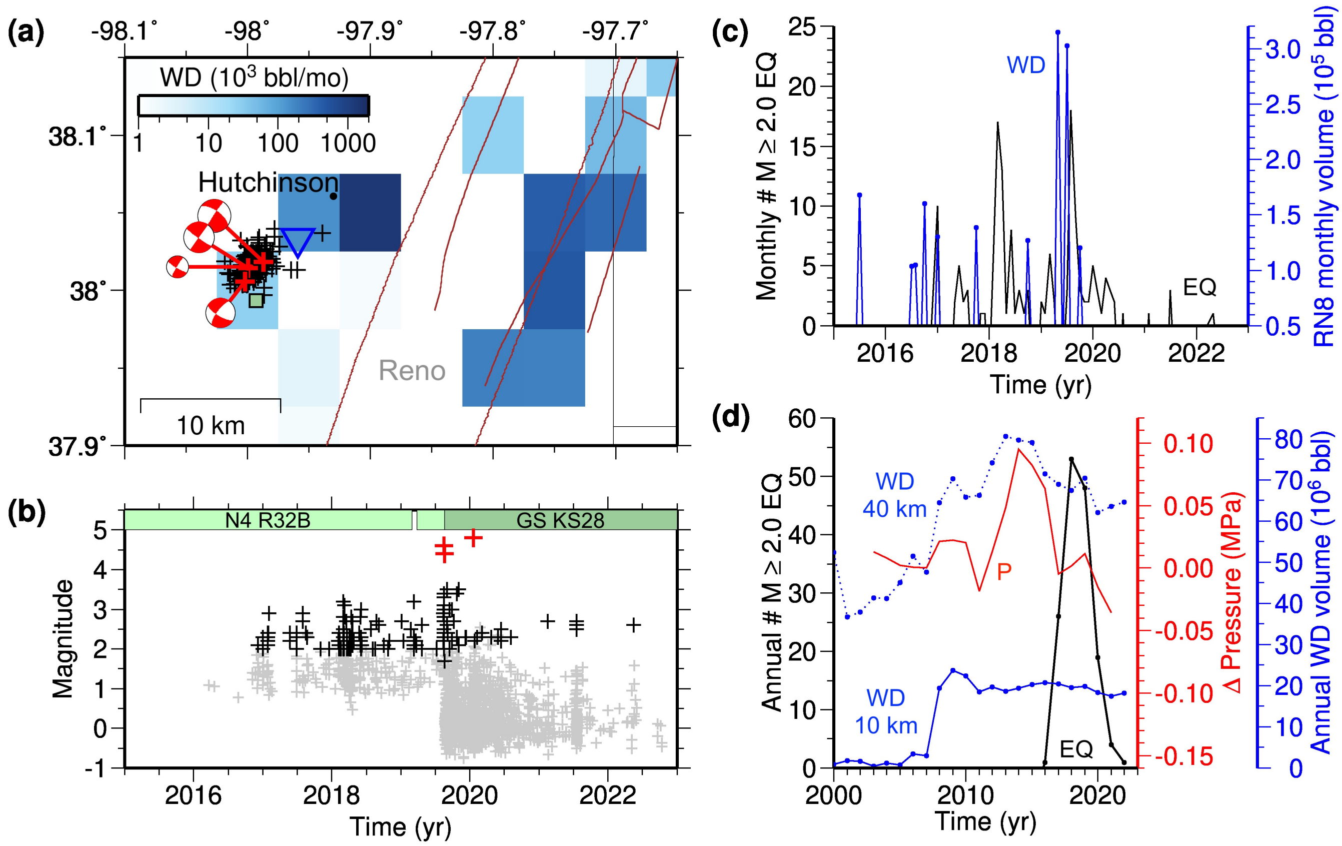

Figure 2 Hutchinson seismicity and WD. (a) Map of earthquakes (crosses, red if M≥4) and average monthly Arbuckle WD volume from 2015 to 2022 computed in 0.05°×0.05° bins. Focal mechanisms are for those earthquakes with USGS fault plane solutions. Blue inverted triangle marks location of Class I well KS-01-155-004 (RN4). Green square denotes seismic station GS KS28 (Supplemental Figure S1b shows N4 R32B, 77 km away). The city of Hutchinson (dot) and counties (gray) are labeled. (b) Magnitude-time plot for template earthquakes (black) and matched events (gray). Bars at top of plot denote timing of stations used for template matching. (c) Monthly rate of M≥2 earthquakes ([EQ], black) and WD volume for Class I well KS-01-155-008 (RN8) (blue). (d) Annual rate of M≥2 earthquakes, annual rate of WD wells within 10 km (solid blue) and 40 km (dotted blue) of seismicity, and annual change in pressure ([P], red) at RN4.

the pressure data for each Class I well to remove random fluctuations and obtain trends in the data (Supplemental Figure S4). We used the pressure trend to calculate the annual change in pressure (Figures 2d and 3e) as several studies have found that pressure rate is the dominant control on seismicity rate (Langenbruch et al., 2018; Ansari et al., 2019; Ansari and Bidgoli, 2021). Data for Class II wells included monthly and annual injection volumes for both SWD and EOR wells. However, there were inconsistencies in the reported injection intervals for Class II wells. Due to the sheer number of EOR wells and the less likelihood of EOR wells generating seismicity, an extensive effort was put forth to clean up only the SWD injection database and identify those injecting into or below the Arbuckle. For simplicity, from here on out we use the term 'Arbuckle' in a general sense to refer to all units from the Arbuckle down the Precambrian basement. See Supplemental Material for details on the quality control conducted and the cleaned dataset of Arbuckle SWD wells (Dataset S4). Data for HF wells included the location and start and end time of HF stimulation while data for production wells included monthly volumes of oil and gas produced. Production volumes are reported by lease, instead of individual wells. Therefore, we were not able to isolate Arbuckle wells for analysis, thus, wells from all intervals were included.

3 Characteristics of Seismicity

3.1 Hutchinson, Kansas

The city of Hutchinson in Reno County is a region where up until late 2016 there had been no recorded earthquakes (Figure 2, Supplemental Figure S1a), yet seismicity greatly increased in 2017 and there were three M≥4 earthquakes within six months of each other in 2019-2020. Earthquakes occurred in a ~5x5 km area, and those with focal mechanisms indicated strike-slip faulting where nodal planes paralleled regional faults (Figure 2a).

Template matching back to February 2014 detected an additional 1,577 earthquakes (~13-fold increase), with the first detected earthquake in early 2016, eight months prior to the first template earthquake (Figure 2b). Maximum earthquake magnitudes were on average M_L 3 up until August 2019 when a M_L 4.6 and M_L 4.4 earthquake occurred two days apart. Five months later, a M_L 4.8 earthquake occurred on 19 January 2020. The 2020

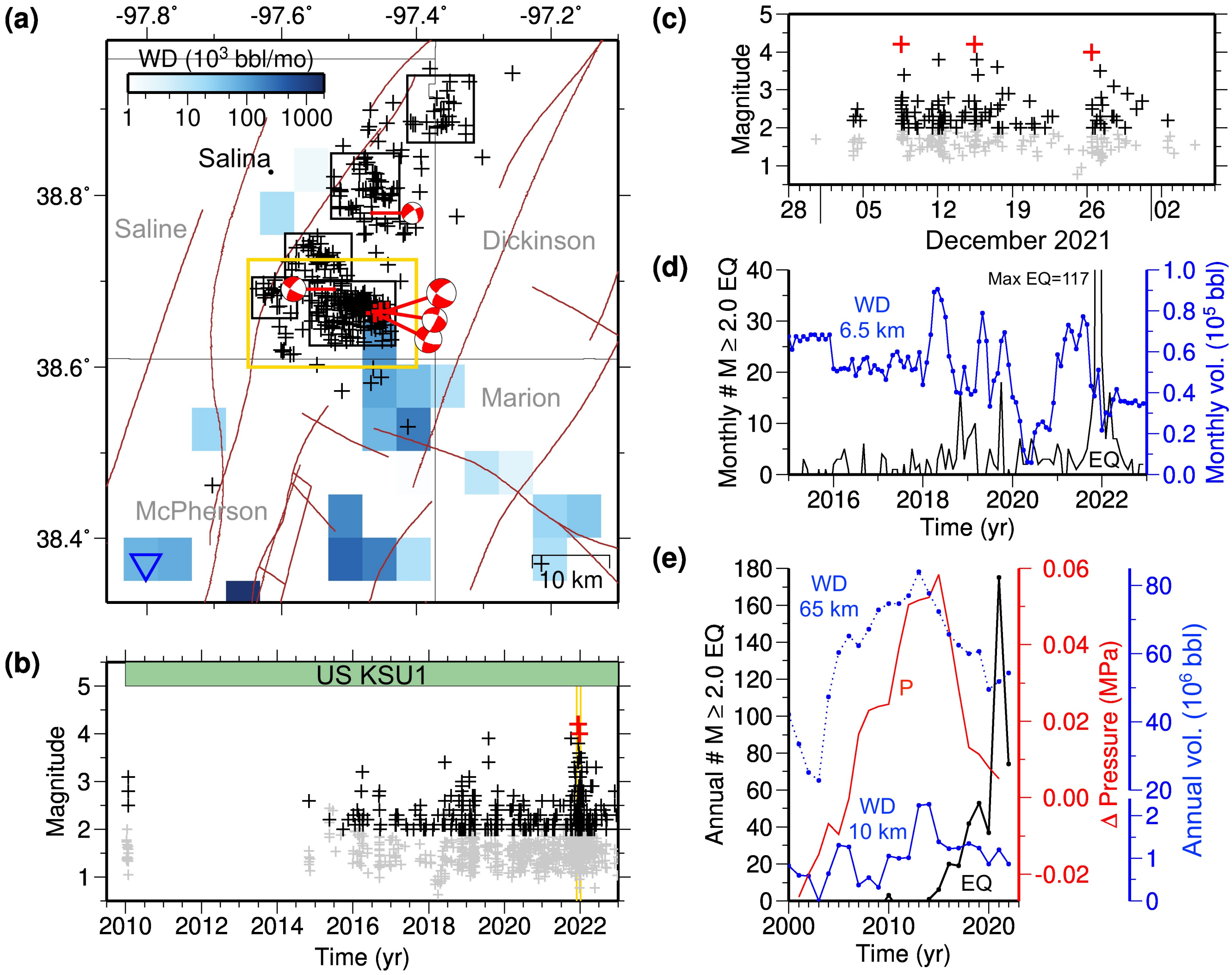

Figure 3 **Salina seismicity and WD**. (a) and (b) are in the same format as Figure 2a, b. Yellow box outlines December 2021 swarm in (c). Black boxes outline regions for which we estimated the CoV. Blue inverted triangle marks location of Class I well KS-01-113-006 (MP6). US KSU1 was outside of the map boundary (60-120 km from template earthquakes; Supplemental Figure S1b). (c) Magnitude-time plot for the December 2021 swarm which resulted in three M≥4 earthquakes. (d) Monthly rate of M≥2 earthquakes (black) and WD volume for the 2 wells within 6.5 km of the 2021 swarm (blue). (e) Annual rate of M≥2 earthquakes (black), annual rate of WD wells within 10 km (solid blue) and 65 km (dotted blue) of the 2021 swarm, and annual change in pressure (red) at MP6. Note the broken scale for WD volume.

M_L 4.8 earthquake was the third largest recorded earthquake in Kansas. Fortunately, with the installation of GS KS28, two days following the second M≥4 earthquake, template matching was able to better capture the aftershock sequences of the M≥4 earthquakes (Supplemental Figure S5). This was especially valuable for the 2020 M_L 4.8 sequence as the next largest magnitude was a M_L 2.2 and the minimum magnitude of the template catalog was a 2.0, making the aftershock sequence non-evident in the previously existing event catalog and highlighting the immense value of nearby seismic stations. Because GS KS28 was not installed until two days following the second M≥4 earthquake, we were not able to assess temporal patterns of seismicity directly prior to these M≥4 earthquakes. However, N4 R32B detected no earthquakes in the month prior. In 2021 and 2022, the annual number of M≥2 earthquakes had decreased such that values were lower than what was observed in the years prior to the M≥4 earthquakes.

3.2 Salina, Kansas

The city of Salina in Saline County is another region where historically there have been no recorded earthquakes, except for a small cluster in January 2010. (Figure 3, Supplemental Figure S1a). More recently, there were three M≥4 events within three weeks of each other in December 2021. Compared to the seismicity in Hutchinson, earthquakes were more spread out across Saline and neighboring counties, occurring in multiple clusters that roughly formed a north-northeast trend (Figure 3a). Those with focal mechanisms mostly indicated strike-slip faulting similar to those in Hutchinson.

Template matching only generated a 3-fold increase in earthquakes (additional 719 events), likely due to the distance of US KSU1 from seismicity (60-120 km). Template matching confirmed a lack of seismic activity be-

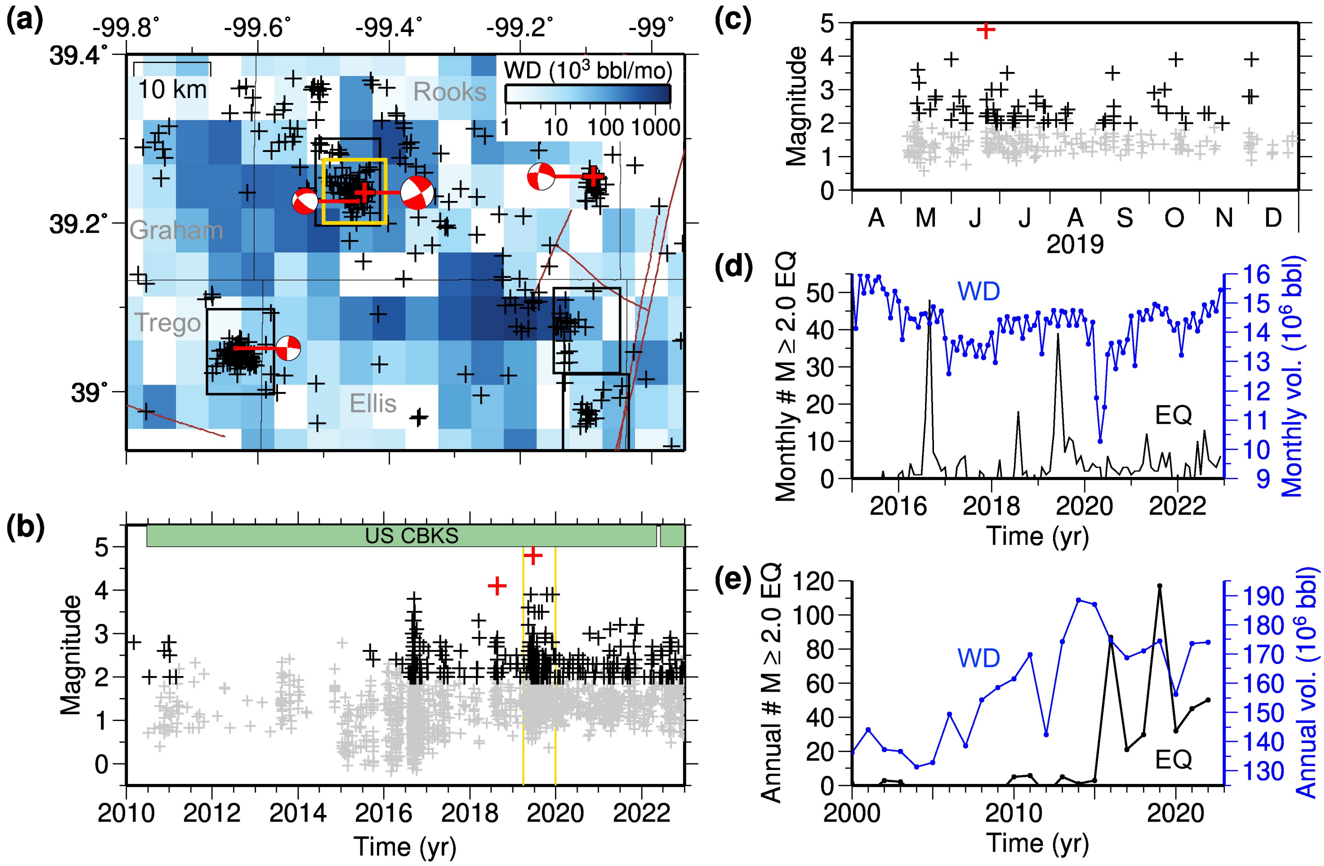

Figure 4 **CKU seismicity and WD**. (a) and (b) are in the same format as Figure 2a, b. Yellow box outlines 2019 swarm in (c). Black boxes outline regions for which we estimated the CoV. US CBKS was outside of the map boundary (18-90 km from template earthquakes; Supplemental Figure S1b). (c) Magnitude-time plot for the 2019 swarm which resulted in a MW 4.8 earthquake. (d) Monthly rates of injected volume for Arbuckle WD wells within 0.1˚ of the map boundary (blue) and M≥2 earthquakes (black). (e) Same as in (d) except annual rates are plotted.

tween the January 2010 cluster and the start of increased seismicity in November 2014 (Figure 3b). While the average monthly rate of M≥2 earthquakes increased to 3 for November 2014 to October 2021, that rate increased by a factor of 6 in November 2021 and a factor of 40 in December 2021. From April 2022 onward, the monthly rate of M≥2 earthquakes had returned to an average of 3. The maximum magnitudes of events had been increasing, culminating in the three M≥4 earthquakes (M 4.2, 4.2 and 4.0) in December 2021 (Figure 3b). The December 2021 cluster behaved more like a swarm than a mainshock-aftershock sequence with multiple events near the maximum magnitude and a lack of Omori decay (Figure 3c).

3.3 Central Kansas Uplift

Historically, the northern region of the CKU was the most seismically active of the regions analyzed in this study (Supplemental Figure S1a). It is notable that a potentially induced earthquake swarm may have occurred in 1989 near the town of Palco in Rooks County. The 1989 swarm, which included a M 3.8 and M 4.0, occurred directly below a WD well (Armbruster et al., 1989). There have been two M≥4 earthquakes since the 1989 M 4.0 earthquake, a M_L 4.1 in August 2018 and M_W 4.8 in June 2019. The 2019 M_W 4.8 earthquake was the second largest recorded earthquake in Kansas and just 10 km from the 1989 M 4.0 potentially WD-induced earthquake. Recent earthquakes generally followed a north-west trend paralleling one of the faults of the CKU with a few pockets of closely clustered earthquakes (Figure 4a). Earthquakes with fault plane solutions indicated predominantly strike-slip faulting.

Template matching increased the number of earthquakes by a factor of 6 (additional 1,723 events) and filled in the gap of seismicity from 2011 to 2016 (Figure 4b). The annual rate of M≥2 earthquakes greatly increased from an average of 2 per year from 2000 to 2015 to an average of 55 per year from 2016 to 2022. The June 2019 M_W 4.8 earthquake occurred during an increase in seismic activity that started about a month prior and lasted about seven months, behaving more like a swarm than a mainshock-aftershock sequence (Figure 4c).

3.4 North-central Kansas: Jewell County

Jewell County and the surrounding area in north-central Kansas, similar to the Hutchinson and Salina regions, typically had little to no earthquakes prior to 2015 (1 earthquake in 2013) and has seen more than one M≥4 earthquake within the last 5 years, a M_L 4.1 in May 2021 and M_L 4.0 in July 2022 (Figure 5). We do note that this region is just to the west of a mapped

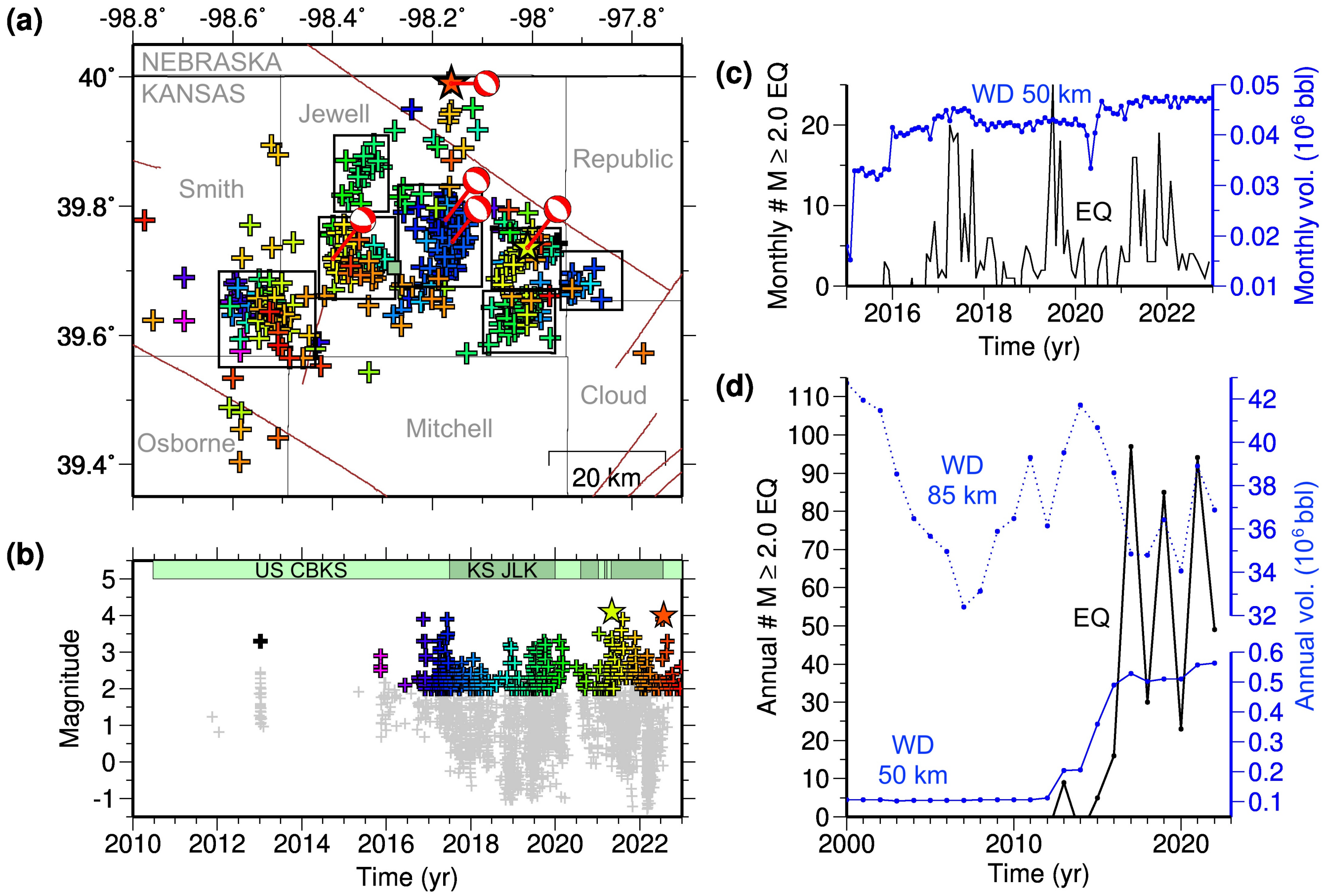

Figure 5 Jewell seismicity and WD. (a) Map of earthquakes (crosses colored by time, star if M≥4). Focal mechanisms are for earthquakes with USGS fault plane solutions. Green square denotes seismic station KS JLK, 2-45 km from template earthquakes (Supplemental Figure S1b shows US CBKS; 119-190 km). Black boxes 1-7 outline regions of seismicity in Supplemental Figure S6 and regions for which we estimated the CoV. (b) Magnitude-time plot for template earthquakes (colored) and matched events (gray). Bars at top of plot denote timing of stations used for template matching. (c) Monthly rate of M≥2 earthquakes (black) and WD volume for Arbuckle wells within 50 km of Region 1 (blue). (d) Same as in (c) but showing the annual rate with the addition of WD volume for Arbuckle wells within 85 km of Region 1 (dotted blue). Note the broken scale for WD volume.

fault that has seen prior seismic activity (Supplemental Figure S1a, Steeples et al., 1990). Fault plane solutions were different from the predominantly strike-slip faulting focal mechanisms observed in Hutchinson, Salina, and the CKU. Focal mechanisms instead indicated northwest-southeast normal faulting, parallel to the regional northwest-southeast trending faults.

Template matching increased the number of earthquakes by a factor of 6 with an additional 1,876 events (Figure 5b). There was a small mainshock-aftershock sequence in January 2013 followed by a lull in seismic activity until late of 2015 when the number of events began increasing.

Spatially, seismicity appeared to cluster into seven main regions (Figure 5a). Regions 1 and 2 have been more active throughout time with several bursts of seismicity beginning in late 2015 and 2018, respectively (Supplemental Figure S6). On the other hand, Regions 4 and 5 each had one period of increased seismicity. These elevated periods of seismicity lasted about eight months and were the only times these regions had M≥3 events. The eight-month period of increased seismicity consisted of several bursts of swarm-like seismicity lasting a couple days to a week (Supplemental Figure S6). Region 6 contained one of the M≥4 earthquakes, a M_L 4.1 in May 2021, whose burst of seismicity lasted two days. The other M≥4 earthquake, M_L 4.0 in July 2022, occurred near the Nebraska border and had no trailing seismicity. The only nearby earthquake was a M_L 2.8 a week prior. There does not appear to be any spatial migration between the seven regions, although we do note that Region 1, which is closest to injection wells, has the earliest detected seismicity (Figure 5a and Supplemental Figure S6).

4 Summary of Seismicity Findings

A comparison of the seismicity findings from the four different regions can be found in Table 1. The primary similarities are in the number of larger earthquakes and the onset of increased seismicity. There is also general agreement in the strike-slip focal mechanisms, with the exception of normal-faulting in Jewell County indicating a potential change in stress field in the northern-

	Hutchinson	Salina	CKU	Jewell
# Earthquakes: M≥4, M≥3	3, 18	3, 28	2, 31	2, 48
First Detected Seismicity	Mar 2016	Jan 2010	Before 2010	Nov 2011
Time of Increased Seismicity	Nov 2016	Jan 2016	Nov 2014	Nov 2015
Focal Mechanism	Strike-slip	Strike-Slip	Strike-Slip	Normal
Factor Increase via Template Matching	6.4x	2.1x	4.2x	3.4x
Distance to Nearest Seismic Station (km)	R32B: 75-80 KS28: 2-6	KSU1: 60-120	CBKS: 18-90	CBKS: 119-190 JLK: 2-45
Magnitude of Completeness (Mc)	0.05	1.55	1.35	1.05
b+ value	0.69	0.78	0.72	0.52
Interevent CoV	3.8	3.7	4.8	5.6
# Wells near M≥4: ≥50K, ≥100K, ≥300K (bbl/m)	<10 km: 3, 3, 2 <40 km: 28, 18, 5	<10 km: 1, 0, 0 <40 km: 11, 7, 3	<10 km: 17, 7, 0 <40 km: 80, 29, 1	<10 km: 0, 0, 0 <40 km: 0, 0, 0*

Table 1 Summary of Seismicity Findings for Each Region. *high-rate wells 80-140 km away

most part of the state. The factor increase from template matching is modest with all regions less than a factor of 10. This is likely due to the relatively large distance to the closest seismic station (and most stations having relatively high noise level), with the lowest factor and highest M_C occurring in Salina when the nearest recordings were entirely in excess of 60 km. In the case of a station within a few kilometers of all of the seismicity (Hutchinson), the factor was highest and the resulting M_C was lowest.

There were also some similarities in the frequency-magnitude distributions, with the b-positive values (0.52 to 0.78; Table 1, Supplemental Figure S3) all lower than what is typically observed for natural earthquakes (∼1.0, e.g., Burridge and Knopoff, 1967). Although there is considerable debate, b-values are traditionally thought to reflect the stress state (Scholz, 1968), and that the low b-values observed in these study regions imply a stress state that is closer to failure (Rivière et al., 2018). One possibility is that the fluid pressures due to WD are driving the fault closer to failure, as some studies have attributed changes in b-values with changes in pressure gradient where the lowest b-values (<1) were often observed during the largest injection rates (Lei et al., 2008; Bachmann et al., 2012; Mousavi et al., 2017).

The CoV values reported in Table 1 were determined by taking the average of all of the CoV values calculated in each of the geographic bins for each of the four regions. The values ranged from 3.8 to 5.6 indicative of relatively high temporal clustering of events (Kagan and Jackson, 1991). These CoV values are within the range of observed CoV of seismicity induced by WD in Kansas, Oklahoma, and Texas (∼1-8, e.g., Schoenball and Ellsworth, 2017b; Cochran et al., 2018; Skoumal et al., 2019, 2020). There is general consensus that low CoV (∼1) is consistent with a steady driving force that prevents earthquake clustering, which could be caused by consistent pore-pressure changes from WD (Cochran et al., 2018; Skoumal et al., 2020). Higher CoV values (>2) would be due to a fault system that is very sensitive to small changes in stress or rapid changes in stress, which could be a sign of a critically stressed fault or HF, respectively (Skoumal et al., 2019, 2020). Since HF is not spatially or temporally associated with the seismicity here (Section 5.1), it implies the larger CoV values are a result of seismicity being induced on critically stressed faults. Cochran et al. (2018) argued that earthquakes further from high-rate injections wells in southern Kansas had smaller pressure perturbations such that earthquake-earthquake interactions can result in more temporal clustering and higher (>2) CoV values. This is consistent with the Delaware Basin of western Texas where the far-field seismicity has some of the highest CoV values (Skoumal et al., 2020). We note that Jewell County, which has the seismicity furthest from high-rate WD, has the highest CoV in our study (Table 1), with strongly clustered seismicity similar to the far-field seismicity of western Texas (Supplemental Figure S7).

5 Relationship Between Seismicity and Industrial Activities

5.1 Lack of Correlation with Extraction, Enhanced Recovery, and Hydraulic Fracturing

It is unlikely that oil and gas production played a significant role in driving the increase in seismicity in the four study regions. Even in the CKU region which had the largest amount of oil extracted, the total was nearly an order of magnitude less than what was being injected into the Arbuckle in the region (c.f., Figure 1b and 6a). Therefore, it was unlikely that injection into the Arbuckle on the CKU was balanced by hydrocarbon production as suggested by Ansari and Bidgoli (2021). In Hutchinson and Salina, oil production was even less significant. The regions of gas production did not coincide spatially with seismicity (Figure 6b), with the most prolific region of gas production in south-west Kansas, far from the seismicity analyzed in this study. Furthermore, most of the induced seismicity has focal mechanisms that are primarily strike-slip while extraction typically induces dip-slip earthquakes (Segall, 1989; McGarr et al., 2002).

HF was ruled out as a driving factor of seismicity in the four study regions due to the lack of spatial and temporal overlap with seismicity. There were a few HF wells in the CKU (6 wells) and Salina (1 well) regions, but the vast majority of HF wells were located in south-west and south-central Kansas far from our focus regions (Figure 6c). In the Salina and CKU regions, there was no seismicity within 10 km of active HF wells. Since HF-induced seismicity typically occurs in close proximity to the HF well (e.g., Schultz et al., 2020), HF is not suspected to be a driving factor for Kansas seismicity.

While there was some spatial overlap between EOR operations and seismicity (Figure 6d), total EOR injection volumes from all intervals were only 40% of the total WD volumes injected into the Arbuckle and EOR wells typically targeted shallower intervals. Furthermore, EOR has a lower likelihood of generating pressure changes large enough to induce seismicity as a significant fraction of the volumes injected for EOR are removed during production which aims to keep the fluid pressure in the reservoir at or below its original level (Rubinstein and Mahani, 2015). However, the relationship between EOR and seismicity is under-studied even though EOR has been proposed to have caused large magnitude seismicity in the Cogdell, TX oil field (Gan and Frohlich, 2013).

Despite the lack of correlation between seismicity and production, HF, and EOR, regions of increased seismicity occurred in close proximity to regions of high WD injected volumes into the Arbuckle, with the curious exception of Jewell County. Next, we dive deeper into the relationship between WD in the Arbuckle and seismicity in the four study regions.

5.2 Hutchinson, Kansas

Of the regions of focus in this study, Hutchinson is the only region which has been previously correlated to WD (Peterie et al., 2018; Ansari et al., 2019; Peterie et al., 2020). Peterie et al. (2020) concluded that Hutchinson seismicity appeared to be a result of combined pressure changes from both local and distant WD. There are three high-rate WD wells in Hutchinson (108,000 to 788,000 barrels per month [bbl/m]) that locally elevated pressures. Class I well RN8, 1 km from Hutchinson seismicity, had variable injection rates with occasional spikes of high-rate injection for several days often exceeding 20,000 bbl/d separated by months with no injection (Figure 2c; Peterie et al., 2020). Class I wells RN9 and RN11, 10 km from Hutchinson seismicity, began injecting at consistently high-rates in 2008 averaging 24,000 bbl/d (Peterie et al., 2020). Since 2016, when seismicity was first detected in Hutchinson, increased rates of seismicity appeared to follow periods of high-rate injection at RN8 (Figure 2c; Peterie et al., 2020). About 3 weeks after shut-in at RN8, the seismicity rate once again increased, and this time included two M≥4 earthquakes. The largest earthquake in Hutchinson and the second largest in Kansas, M4.8, occurred five months following shut-in at RN8. Other studies have observed the largest event to occur following shutdown (Healy et al., 1968; Segall and Lu, 2015).

We looked at cumulative volume injected with respect to distance from Class I wells in Hutchinson which had pressure data. Pressure gradient did not correlate with annual volume of local wells but did when considering wells up to 40 km away (Figure 2d). However, the onset of seismicity correlated better with maximum pressure than max pressure gradient (Supplemental Figure S4a). Several studies have found that pressure rate is the dominant control on seismicity rate (Langenbruch et al., 2018; Ansari et al., 2019; Ansari and Bidgoli, 2021). Seismicity was first detected two years following the largest pressure increase (Figure 2d). If we assume most of the earthquakes in Hutchinson are occurring in the basement as in south-central Kansas, the delay between the onset of seismicity and large pressure increase may be due to the permeability contrasts between the Arbuckle and the basement. The permeability contrast would delay the onset of pressure propagation to hypocentral depths which takes years to exceed a critical pressure to induce fault failure (Schoenball et al., 2018).

While results from this study agree with Peterie et al. (2020) that local and distal injection is necessary to explain pressure changes in Hutchinson, we did not find it necessary to include WD wells out to 90 km. We found that by including wells out to 40 km we started to see pressure rate increases coincide with increases in injection volume (Figure 2d).

5.3 Salina, Kansas

There were no large-rate WD wells within 10 km of the December 2021 swarm. However, there were two wells 0.5 km from each other and about 6.5 km from the December 2021 swarm where when combined there were three several month-long periods of injection exceeding 70,000 bbl/m (Figure 3d). Similar to what was observed in Hutchinson, peaks in seismicity followed peaks in monthly injection volumes of nearby wells by 4-6 months (Figure 3d). We note that wells near the December 2021 swarm were about 30 km from the furthest cluster of Salina earthquakes to the north. The three clusters did not overlap with regions of WD suggesting regional wells may have had a larger influence on generating seismicity in those areas. With regards to the December 2021 swarm having nearly an order of magnitude more M2 earthquakes than the other Salina swarms, we suspect this may be due to variable fault conditions.

Unfortunately, the closest Class I well to the December 2021 swarm was about 43 km to the south in McPherson County. Therefore, we utilized the pressure data from that well as a rough estimation of Arbuckle formation pressure near Salina (Supplemental Figure S4b). As observed in Hutchinson, pressure gradient did not correlate with annual volume of local wells but did when considering wells further away, albeit at a further distance (65 km, Figure 3e). The onset of increased seismicity in Salina correlated better with maximum pressure than max pressure gradient, another similarity to Hutchinson (Supplemental Figure S4b).

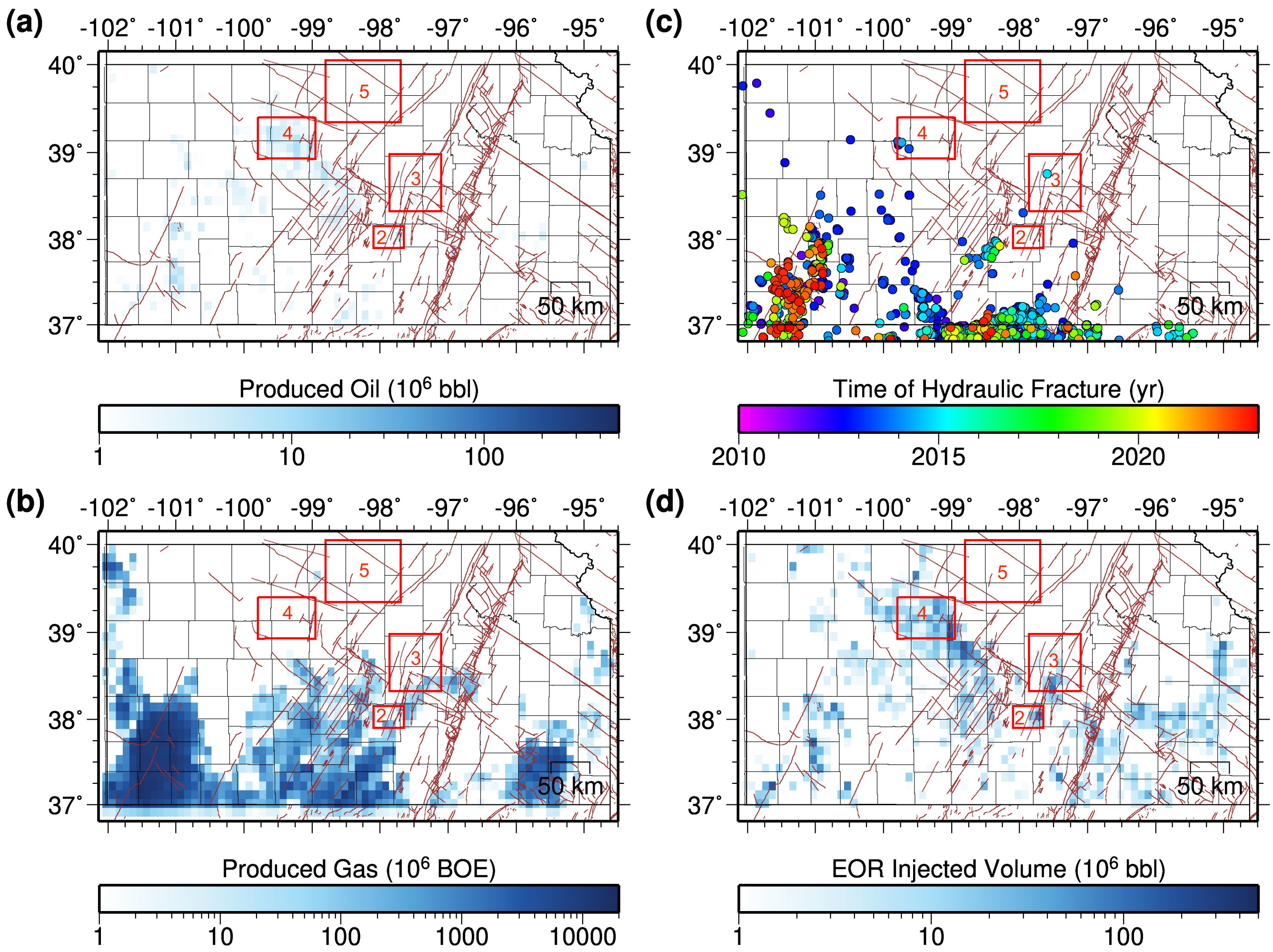

Figure 6 Maps of other industrial operations in Kansas from 2000 to 2022. Red boxes mark the four focus regions in this study corresponding to Figures 2-5. (a) Total amount of oil produced from all intervals computed in bins that are 0.1°×0.1°. (b) Total amount of gas produced (shown in barrels of oil equivalent [BOE]) from all intervals computed in bins that are 0.1°×0.1°. (c) HF wells (circles) colored by time of stimulation. (d) Total volume from EOR wells targeting all intervals computed in bins that are 0.1°×0.1°. Note oil and EOR wells are colored at the same scale as WD injection in Figure 1b.

5.4 Central Kansas Uplift

A majority of CKU seismicity (82%) occurred within 10 km of large-volume WD wells (≥50,000 bbl/m). This region had a higher spatial density of large-volume WD wells compared to the other regions we analyzed. The 2019 M_W 4.8 earthquake was within 10 km of 7 wells injecting over an average monthly rate of 100,000 bbl/m. Given the larger spatial spread of seismicity in this region it was difficult to define local and regional wells. Therefore, when calculating total monthly and annual volumes we considered all wells within 0.1° of the bounds of Figure 4. There was no clear correlation between monthly seismicity and monthly injection volume (Figure 4d). This could be due to the larger area over which wells are injecting on the CKU. The annual injection rate gradually increased from 2005 to 2014, remained elevated in 2015 and then dropped from 2016 to 2017 (Figure 4e). From 2018 to 2022 injection rate was on a small upward trend except for a sharp decrease in 2020. Maximums in annual earthquakes in 2016 and 2019 lagged two years and occurred during maximums in annual injection rates, respectively.

Even though WD wells in the CKU region have injected nearly twice the amount of fluids into the Arbuckle from 2000 to 2022 as wells in a similar sized area of Harper and Sumner counties (3,598 million vs 1,732 million bbls), the Harper-Sumner region saw six times the amount of M≥2 earthquakes during this time compared to the CKU region (Supplemental Figure S8). While this difference could be explained by a variety of factors such as differences in fault conditions or preexisting stresses, we suspect the time over which injection occurred could have had an important role as the Harper-Sumner region experienced a much larger increase in injection rate compared to the relatively gradual increase the CKU experienced.

5.5 North-central Kansas: Jewell County

The nature of the seismicity in Jewell County and the surrounding regions is intriguing as the number of M≥2 earthquakes has greatly increased since late 2016. The increased seismicity is unlikely due to natural causes, although there was no industrial activity such as WD, production, EOR, or HF, within 40 km (Figure 1b, Figure 6). Nor was there injection nearby across the border in Nebraska (Figure 1b). Seismicity was ∼80-140 km from high-rate injection on the CKU. However, there were three disposal wells ∼45 km from Region 1, the closest cluster to the CKU, and ∼90 km from the furthest earthquake. While individually these wells had a low average monthly injection rate of 4,900 to 26,000 bbl/m, the total annual volume of wells within 50 km from Region 1 showed that annual volumes had increased twofold in 2013, the same year as the first earthquake cluster of earthquakes in Region 6 (Figure 5d). The largest earthquake rate increase coincided with a five-fold increase in annual volume in 2017, relative to 2012. While maximums in annual volumes overlapped with peaks in seismicity, this was not as clearly seen on the monthly scale (Figure 5c). Total monthly volumes from the three closest WD wells were quite small compared to other areas in Kansas and may not be large enough to generate the pressure increases necessary for inducing seismicity in this region. Therefore, we included wells within 85 km of Region 1 to include the high-rate wells on the CKU. The first large spike in seismicity followed a maximum in injection rate by three years and subsequent spikes in seismicity overlapped with relative injection rate maximums (Figure 5d).

The more continuous seismic activity of Regions 1 and 2, those closest to CKU injection, could suggest that these regions are more fluid driven than regions that are further away and exhibit more sporadic seismic activity (Supplemental Figure S6). Verdecchia et al. (2021) came to a similar conclusion for the 2014 M 4.6 Harper and 2014 M 4.9 Milan sequences where the Harper sequence displayed more continuous behavior and occurred closer to several large injection wells while the Milan sequence was characterized by more episodic activity and occurred more than 50 km from a major disposal well. Verdecchia et al. (2021) suggested fluid diffusion has a larger influence on controlling seismicity clusters closer to large injection wells whereas earthquake interactions may play a bigger role in the evolution of sequences at greater distances. Additional support for CKU injection influencing seismicity over 50 km away is that the onset of increased seismicity in Jewell County appears to be delayed 1-2 years from the onset of increased seismicity on the CKU supporting the notion of a pressure front migration out from CKU high-rate injection zone.

We believe the seismicity in this region is a prime example of the importance of large distal wells and the potential for far-field pressure diffusion. The minimum distance between CKU injection and Jewell County (∼45 km Region 1) is similar to the distance between northern Harper County and northern Oklahoma where the densest region of high-rate wells is. Similarly long distances of injection-related triggering of seismicity have been proposed in Oklahoma and Texas (Goebel et al., 2017; Skoumal et al., 2020). A global compilation of injection induced seismicity suggested that steady injection above basement into sedimentary layers resulted in a larger spatial footprint of seismicity owing to more efficient pressure and stress transmission (Goebel and Brodsky, 2018). CKU injection occurs into the Arbuckle, which has very high permeabilities and diffusivities (Dempsey and Riffault, 2019; Zhai et al., 2019). Therefore, we propose that the Jewell County seismicity is caused by efficient transmission of fluid pressures from the dense region of high-rate wells in CKU to highly sensitive, critically stressed faults in Jewell County.

6 Implications and Sources of Uncertainty

Results from this study are also important for reconsidering the seismic hazard in Kansas. Induced earthquakes are not included in the traditional National Seismic Hazard Model as they are thought of as temporary features of seismicity, and a short-term (1 year) model forecast that includes induced seismicity has not been issued since 2018 (Petersen et al., 2023). Since induced seismicity has been occurring in several areas of Kansas for nearly a decade, it is important to consider the hazard of the increased seismicity rates. Although much of the seismicity has occurred in rural areas, clusters of seismicity are not far from the larger population centers of Wichita, Hutchinson, and Salina. Magnitudes approaching 5.0 pose considerable hazard to local communities, so a regulatory strategy should be considered going forward (Schultz et al., 2021; Buchanan et al., 2023). We have used an observational approach to demonstrate far-field fluid pressure diffusion is primarily responsible for influencing seismicity in northern and central Kansas. We recommend future studies seek to develop statewide fluid pressure models to evaluate the relative contributions of local and distal WD and explore whether seismicity forecasts can be developed to relate the fluid pressure changes with seismicity rates over time (e.g., Langenbruch et al., 2018; Dempsey and Riffault, 2019; Zhai et al., 2019). In order to inform the regulatory framework, it will be important to assess which configurations of WD wells have a larger influence: a single local high rate well, multiple local moderate rate wells but large cumulative volume wells, multiple regional high rate or large volume wells, or some combination of these scenarios.

Given the limited number of seismic stations in northern and central Kansas, our study indicates more local seismic stations are needed to better locate seismicity and better characterize the faults hosting these earthquakes. Depths of cataloged earthquakes in northern and central Kansas are not well constrained due to the sparse station coverage, so we do not know whether earthquakes occurred in the crystalline basement below the Arbuckle similar to those in southern Kansas (Rubinstein et al., 2018; Schoenball and Ellsworth, 2017a), or in the shallower sedimentary layers (Currie et al., 2018; Kozłowska et al., 2018; Skoumal et al., 2020).

We also note that the Arbuckle has been proposed as a target for carbon sequestration in Kansas (Holubnyak et al., 2017; Schwab et al., 2017), thus this study has large implications for operators in Kansas or in other states as they decide where and which interval to inject CO_2. The strong evidence in our study of far-field forcing from distances >50 km and likely from upwards of 100 km from large volume WD wells implies a large spatial influence from the proposed large volume carbon sequestration in the Arbuckle. Moreover, the heterogenous locations of where seismicity has occurred relative to WD wells indicates the locations of induced seismicity is likely controlled by preexisting unknown structures and prestresses that would be difficult to know in advance of large volume injection. So as operators decide where to inject, they need to not just consider nearby disposal activity, but should take into account regional WD activity. With the large volumes expected for carbon sequestration to be economic, it further highlights the need for and importance of increased seismic monitoring. Investing in increased monitoring in advance would also enable better investigations into the current seismicity that could confirm or refute aseismic regions in Kansas where large WD volumes have already been injected into the Arbuckle.

7 Conclusions

In northern and central Kansas there was about a 2–3-year delay of the onset of the large increase of M≥3.5 earthquakes compared to southern Kansas (Figure 1a). While two-thirds of Kansas seismicity occurred near the Kansas-Oklahoma border and southern Kansas seismicity rates had been decreasing since 2018, northern and central Kansas had seen a rapid rise of M≥3.5 earthquakes since 2019. For nearly three decades, there had been no M≥4.0 earthquakes recorded in northern and central Kansas. However, from 2019 to 2022, there had been ten M≥4.0 earthquakes in northern and central Kansas, including two M 4.8 events. Southern Kansas had only one M≥4.0 earthquake in this time. Seismic activity in Hutchinson and Salina has decreased in 2022 but has remained elevated in the CKU and Jewell County.

For the Hutchinson, Salina, and CKU regions, we suggest the long history of injection into the Arbuckle raised fluid pressures on nearby faults until the effective stress was reduced enough such that the critically stressed faults required only small increases in fluid pressure from local disposal wells to induce seismicity (Ansari and Bidgoli, 2021). Due to the spatial density of high-rate wells in the CKU region, we suspect local wells may have more of an influence on generating seismicity compared to Hutchinson and Salina regions where more distal wells are believed to influence seismicity. As for the perplexing case in Jewell County, we propose that the seismicity is caused by efficient transmission of fluid pressures from the dense region of high-rate wells in the CKU to highly sensitive, critically stressed faults in Jewell County. Our study agrees with several prior studies showing that perturbations of the stress field due to fluid injection can have a far-reaching impact on seismicity (Keranen et al., 2014; Goebel et al., 2017; Ansari et al., 2019; Zhai et al., 2020; Ansari and Bidgoli, 2021; Haddad and Eichhubl, 2022).

The degree to which local and/or distant fluid pressure changes are primarily responsible for seismicity may differ by region depending on historical injection in the region and the number and spacing of large volume WD wells. We recommend hydromechanical modeling studies would be able to give more insight into the relative contributions of local and regional wells to Kansas seismicity.

Acknowledgements

This work was supported by funds from the University of Kansas (KU) Dean A. McGee Professorship in Applied Geophysics. Part of this work was performed at the HPC facilities operated by the Center for Research Computing at KU supported in part through the NSF MRI Award #2117449. IRIS Data Services used in this study are funded through the Seismological Facilities for the Advancement of Geoscience (SAGE) Award of the NSF under Cooperative Support Agreement EAR-1851048. We thank editor, Y. J. Tan, and two anonymous reviewers for their constructive and detailed reviews.

Data and code availability

Earthquakes in Kansas from January 2000 through December 2022 were obtained from the KGS (https://www.kgs.ku.edu/Geophysics/Earthquakes/data.html; last accessed March 2023) and the ANSS Comprehensive Catalog (https://earthquake.usgs.gov/data; last accessed July 2023). Seismic waveform data from the GS (Albuquerque Seismological Laboratory (ASL)/USGS, 1980), N4 (Albuquerque Seismological Laboratory/USGS, 2013), and US (Albuquerque Seismological Laboratory (ASL)/USGS, 1990) networks were obtained from the Incorporated Research Institutions for Seismology (now EarthScope Consortium) Data Management Center Web Services (IRIS DMC) (http://service.iris.edu/fdsnws/dataselect/1/). Waveform data for KS JLK was accessed upon request from the KGS. Kansas Class II (SWD and EOR) well data was downloaded from the KGS (https://www.kgs.ku.edu/Magellan/Qualified/class2_db.html; last accessed June 2023). Oklahoma Class II SWD well data from 2005-2017 was obtained from Skoumal et al. (2018) and data from 2018-2022 was downloaded from the OCC (https://oklahoma.gov/occ/divisions/oil-gas/oil-gas-data.html; last accessed June 2023). Nebraska Class II SWD well locations were downloaded from the Nebraska Oil and Gas Conservation Commission (http://www.nogcc.ne.gov/Publications/NebraskaWellData.zip; last accessed February 2024). Kansas Class I well data was obtained from multiple sources. Annual volumes for 2000-2009 and annual formation pressures for 2000-2017 were provided in Ansari et al. (2019); monthly volumes for 2010-2018 and annual formation pressure for 2018-2021 were available upon request from the KDHE; monthly volumes for 2019-2022 were downloaded from the KGS (http://maps.kgs.ku.edu/kgs_web/injection/class1_permits.cfm; last accessed June 2023). Kansas oil and gas production data were obtained from the KGS (http://www.kgs.ku.edu/Magellan/Field/lease.html; last accessed July 2023). Hydraulic fracture well data were retrieved from FracFocus (http://fracfocus.org/; last accessed April 2022).

The Supplemental Material provides further details on the methods and well data used in this study as well as additional figures supporting the main text. The Supplemental Material includes the template matched catalog (Dataset S1), compiled Class I injection (Dataset S2) and pressure (Dataset S3) data, and manually corrected Class II Arbuckle SWD injection data (Dataset S4).

Competing Interests

The authors have no competing interests.

References

Albuquerque Seismological Laboratory (ASL)/USGS. US Geological Survey Networks [Data set], 1980. doi: 10.7914/SN/GS.

Albuquerque Seismological Laboratory (ASL)/USGS. United States National Seismic Network [Data set], 1990. doi: 10.7914/SN/US.

Albuquerque Seismological Laboratory/USGS. Central and Eastern US Network [Data set], 2013. doi: 10.7914/SN/N4.

Ansari, E. and Bidgoli, T. S. Precambrian Crystalline Basement Properties From Pressure History Matching and Implications for Induced Seismicity in the US Midcontinent. *Geochemistry, Geophysics, Geosystems*, 22(8), Aug. 2021. doi: 10.1029/2021gc009660.

Ansari, E., Bidgoli, T. S., and Hollenbach, A. Accelerated Fill-Up of the Arbuckle Group Aquifer and Links to U.S. Midcontinent Seismicity. *Journal of Geophysical Research: Solid Earth*, 124(3): 2670–2683, Mar. 2019. doi: 10.1029/2018jb016926.

Armbruster, J., Steeples, D., and Seeber, L. The 1989 earthquake sequence near Palco. Kansas: A possible example of induced seismicity (abstract. *Seismological Research Letters*, 60(4):141, 1989.

Bachmann, C. E., Wiemer, S., Goertz-Allmann, B. P., and Woessner, J. Influence of pore-pressure on the event-size distribution of induced earthquakes. *Geophysical Research Letters*, 39(9), May 2012. doi: 10.1029/2012gl051480.

Bender, B. Maximum likelihood estimation of b values for magnitude grouped data. *Bulletin of the Seismological Society of America*, 73(3):831–851, June 1983. doi: 10.1785/bssa0730030831.

Beyreuther, M., Barsch, R., Krischer, L., Megies, T., Behr, Y., and Wassermann, J. ObsPy: A Python Toolbox for Seismology. *Seismological Research Letters*, 81(3):530–533, May 2010. doi: 10.1785/gssrl.81.3.530.

Buchanan, R. C., Hoffman, R., and Cochran, M. *Induced seismicity in Kansas: Events and responses*, page 27–35. Geological Society of America, May 2023. doi: 10.1130/2023.2559(03).

Burridge, R. and Knopoff, L. Model and theoretical seismicity. *Bulletin of the Seismological Society of America*, 57(3):341–371, June 1967. doi: 10.1785/bssa0570030341.

Choy, G. L., Rubinstein, J. L., Yeck, W. L., McNamara, D. E., Mueller, C. S., and Boyd, O. S. A Rare Moderate-Sized (Mw 4.9) Earthquake in Kansas: Rupture Process of the Milan, Kansas, Earthquake of 12 November 2014 and Its Relationship to Fluid Injection. *Seismological Research Letters*, 87(6):1433–1441, Sept. 2016. doi: 10.1785/0220160100.

Cochran, E. S., Ross, Z. E., Harrington, R. M., Dougherty, S. L., and Rubinstein, J. L. Induced Earthquake Families Reveal Distinctive Evolutionary Patterns Near Disposal Wells. *Journal of Geophysical Research: Solid Earth*, 123(9):8045–8055, Sept. 2018. doi: 10.1029/2018jb016270.

Currie, B. S., Free, J. C., Brudzinski, M. R., Leveridge, M., and Skoumal, R. J. Seismicity Induced by Wastewater Injection in Washington County, Ohio: Influence of Preexisting Structure, Regional Stress Regime, and Well Operations. *Journal of Geophysical Research: Solid Earth*, 123(5):4123–4140, May 2018. doi: 10.1002/2017jb015297.

Davis, S. D. and Frohlich, C. Did (Or Will) Fluid Injection Cause Earthquakes? - Criteria for a Rational Assessment. *Seismological Research Letters*, 64(3–4):207–224, July 1993. doi: 10.1785/gssrl.64.3-4.207.

Dempsey, D. and Riffault, J. Response of Induced Seismicity to Injection Rate Reduction: Models of Delay, Decay, Quiescence, Recovery, and Oklahoma. *Water Resources Research*, 55(1): 656–681, Jan. 2019. doi: 10.1029/2018wr023587.

Ellsworth, W. L. Injection-Induced Earthquakes. *Science*, 341 (6142), July 2013. doi: 10.1126/science.1225942.

Franseen, E. K., Byrnes, A. P., Cansler, J. R., Steinhauff, D. M., and Carr, T. R. The Geology of Kansas—Arbuckle Group. *Current Research in Earth Sciences*, page 1–43, Dec. 2004. doi: 10.17161/cres.v0i250.11789.

Gan, W. and Frohlich, C. Gas injection may have triggered earthquakes in the Cogdell oil field, Texas. *Proceedings of the National Academy of Sciences*, 110(47):18786–18791, Nov. 2013. doi: 10.1073/pnas.1311316110.

Goebel, T., Weingarten, M., Chen, X., Haffener, J., and Brodsky, E. The 2016 Mw5. 1 Fairview, Oklahoma earthquakes: Evidence for long-range poroelastic triggering at >40 km from fluid disposal wells. *Earth and Planetary Science Letters*, 472:50–61, Aug. 2017. doi: 10.1016/j.epsl.2017.05.011.

Goebel, T. H. W. and Brodsky, E. E. The spatial footprint of injection wells in a global compilation of induced earthquake sequences. *Science*, 361(6405):899–904, Aug. 2018. doi: 10.1126/science.aat5449.

Haddad, M. and Eichhubl, P. Fault Reactivation in Response to Saltwater Disposal and Hydrocarbon Production for the Venus, TX, Mw 4.0 Earthquake Sequence. *Rock Mechanics and Rock Engineering*, 56(3):2103–2135, Dec. 2022. doi: 10.1007/s00603-022-03083-4.

Healy, J. H., Rubey, W. W., Griggs, D. T., and Raleigh, C. B. The Denver Earthquakes. *Science*, 161(3848):1301–1310, Sept. 1968. doi: 10.1126/science.161.3848.1301.

Hearn, E. H., Koltermann, C., and Rubinstein, J. L. Numerical Models of Pore Pressure and Stress Changes Along Basement Faults Due to Wastewater Injection: Applications to the 2014 Milan, Kansas Earthquake. *Geochemistry, Geophysics, Geosystems*, 19 (4):1178–1198, Apr. 2018. doi: 10.1002/2017gc007194.

Holubnyak, Y., Williams, E., Watney, L., Bidgoli, T., Rush, J., FazelAlavi, M., and Gerlach, P. Calculation of CO2 Storage Capacity for Arbuckle Group in Southern Kansas: Implications for a Seismically Active Region. *Energy Procedia*, 114:4679–4689, July 2017. doi: 10.1016/j.egypro.2017.03.1599.

Kagan, Y. Y. and Jackson, D. D. Long-Term Earthquake Clustering. *Geophysical Journal International*, 104(1):117–134, Jan. 1991. doi: 10.1111/j.1365-246x.1991.tb02498.x.

Keranen, K. M., Savage, H. M., Abers, G. A., and Cochran, E. S. Potentially induced earthquakes in Oklahoma, USA: Links between wastewater injection and the 2011 Mw 5.7 earthquake sequence. *Geology*, 41(6):699–702, June 2013. doi: 10.1130/g34045.1.

Keranen, K. M., Weingarten, M., Abers, G. A., Bekins, B. A., and Ge, S. Sharp increase in central Oklahoma seismicity since 2008 induced by massive wastewater injection. *Science*, 345(6195): 448–451, July 2014. doi: 10.1126/science.1255802.

Kozłowska, M., Brudzinski, M. R., Friberg, P., Skoumal, R. J., Baxter, N. D., and Currie, B. S. Maturity of nearby faults influences seismic hazard from hydraulic fracturing. *Proceedings of the National Academy of Sciences*, 115(8), Feb. 2018. doi: 10.1073/pnas.1715284115.

Langenbruch, C., Weingarten, M., and Zoback, M. D. Physics-based forecasting of man-made earthquake hazards in Oklahoma and Kansas. *Nature Communications*, 9(1), Sept. 2018. doi: 10.1038/s41467-018-06167-4.

Lei, X., Yu, G., Ma, S., Wen, X., and Wang, Q. Earthquakes induced by water injection at ∼3 km depth within the Rongchang gas field, Chongqing, China. *Journal of Geophysical Research: Solid Earth*, 113(B10), Oct. 2008. doi: 10.1029/2008jb005604.

McGarr, A., Simpson, D., and Seeber, L. *40 Case histories of induced and triggered seismicity*, page 647–661. Elsevier, 2002. doi: 10.1016/s0074-6142(02)80243-1.

Mohammadi, S., Hollenbach, A. M., Goldstein, R. H., Möller, A., and Burberry, C. M. Controls on Timing of Hydrothermal Fluid Flow in South-Central Kansas, North-Central Oklahoma, and the Tri-State Mineral District. *Midcontinent Geoscience*, 3, Aug. 2022. doi: 10.17161/mg.v3i.16812.

Mousavi, S. M., Ogwari, P. O., Horton, S. P., and Langston, C. A. Spatio-temporal evolution of frequency-magnitude distribution and seismogenic index during initiation of induced seismicity at Guy-Greenbrier, Arkansas. *Physics of the Earth and Planetary Interiors*, 267:53–66, June 2017. doi: 10.1016/j.pepi.2017.04.005.

Peterie, S. L., Miller, R. D., Intfen, J. W., and Gonzales, J. B. Earthquakes in Kansas Induced by Extremely Far-Field Pressure Diffusion. *Geophysical Research Letters*, 45(3):1395–1401, Feb. 2018. doi: 10.1002/2017gl076334.

Peterie, S. L., Miller, R. D., Wilson, B. B., and Newell, K. D. Potential factors contributing to induced seismicity near Hutchinson, Kansas. In *SEG Technical Program Expanded Abstracts 2020*, page 1309–1313. Society of Exploration Geophysicists, Sept. 2020. doi: 10.1190/segam2020-3424384.1.

Petersen, M. D., Shumway, A. M., Powers, P. M., Field, E. H., Moschetti, M. P., Jaiswal, K. S., Milner, K. R., Rezaeian, S., Frankel, A. D., Llenos, A. L., Michael, A. J., Altekruse, J. M., Ahdi, S. K., Withers, K. B., Mueller, C. S., Zeng, Y., Chase, R. E., Salditch, L. M., Luco, N., Rukstales, K. S., Herrick, J. A., Girot, D. L., Aagaard, B. T., Bender, A. M., Blanpied, M. L., Briggs, R. W., Boyd, O. S., Clayton, B. S., DuRoss, C. B., Evans, E. L., Haeussler, P. J., Hatem, A. E., Haynie, K. L., Hearn, E. H., Johnson, K. M., Kortum, Z. A., Kwong, N. S., Makdisi, A. J., Mason, H. B., McNamara, D. E., McPhillips, D. F., Okubo, P. G., Page, M. T., Pollitz, F. F., Rubinstein, J. L., Shaw, B. E., Shen, Z.-K., Shiro, B. R., Smith, J. A., Stephenson, W. J., Thompson, E. M., Thompson Jobe, J. A., Wirth, E. A., and Witter, R. C. The 2023 US 50-State National Seismic Hazard Model: Overview and implications. *Earthquake Spectra*, 40(1):5–88, Dec. 2023. doi: 10.1177/87552930231215428.

Rivière, J., Lv, Z., Johnson, P., and Marone, C. Evolution of b-value during the seismic cycle: Insights from laboratory experiments on simulated faults. *Earth and Planetary Science Letters*, 482: 407–413, Jan. 2018. doi: 10.1016/j.epsl.2017.11.036.

Rubinstein, J. L. and Mahani, A. B. Myths and Facts on Wastewater Injection, Hydraulic Fracturing, Enhanced Oil Recovery, and Induced Seismicity. *Seismological Research Letters*, 86(4): 1060–1067, June 2015. doi: 10.1785/0220150067.

Rubinstein, J. L., Ellsworth, W. L., and Dougherty, S. L. The 2013–2016 Induced Earthquakes in Harper and Sumner Counties, Southern Kansas. *Bulletin of the Seismological Society of America*, 108(2):674–689, Feb. 2018. doi: 10.1785/0120170209.

Schaff, D. P. and Richards, P. G. Improvements in magnitude precision, using the statistics of relative amplitudes measured by cross correlation. *Geophysical Journal International*, 197(1): 335–350, Jan. 2014. doi: 10.1093/gji/ggt433.

Schoenball, M. and Ellsworth, W. L. Waveform-Relocated Earthquake Catalog for Oklahoma and Southern Kansas Illuminates the Regional Fault Network. *Seismological Research Letters*, 88 (5):1252–1258, July 2017a. doi: 10.1785/0220170083.

Schoenball, M. and Ellsworth, W. L. A Systematic Assessment of the Spatiotemporal Evolution of Fault Activation Through Induced Seismicity in Oklahoma and Southern Kansas. *Journal of Geophysical Research: Solid Earth*, 122(12), Dec. 2017b. doi: 10.1002/2017jb014850.

Schoenball, M., Walsh, F. R., Weingarten, M., and Ellsworth, W. L. How faults wake up: The Guthrie-Langston, Oklahoma earthquakes. *The Leading Edge*, 37(2):100–106, Feb. 2018. doi: 10.1190/tle37020100.1.

Scholz, C. H. The frequency-magnitude relation of microfracturing in rock and its relation to earthquakes. *Bulletin of the Seismological Society of America*, 58(1):399–415, Feb. 1968. doi: 10.1785/bssa0580010399.

Schultz, R., Skoumal, R. J., Brudzinski, M. R., Eaton, D., Baptie, B., and Ellsworth, W. Hydraulic Fracturing-Induced Seismicity. *Reviews of Geophysics*, 58(3), July 2020. doi: 10.1029/2019rg000695.

Schultz, R., Beroza, G. C., and Ellsworth, W. L. A Strategy for Choosing Red-Light Thresholds to Manage Hydraulic Fracturing Induced Seismicity in North America. *Journal of Geophysical Research: Solid Earth*, 126(12), Dec. 2021. doi: 10.1029/2021jb022340.

Schwab, D. R., Bidgoli, T. S., and Taylor, M. H. Characterizing the Potential for Injection-Induced Fault Reactivation Through Subsurface Structural Mapping and Stress Field Analysis, Wellington Field, Sumner County, Kansas. *Journal of Geophysical Research: Solid Earth*, 122(12), Dec. 2017. doi: 10.1002/2017jb014071.

Segall, P. Earthquakes triggered by fluid extraction. *Geology*, 17(10):942, 1989. doi: 10.1130/0091-7613(1989)017<0942:etbfe>2.3.co;2.

Segall, P. and Lu, S. Injection-induced seismicity: Poroelastic and earthquake nucleation effects. *Journal of Geophysical Research: Solid Earth*, 120(7):5082–5103, July 2015. doi: 10.1002/2015jb012060.

Skoumal, R. J., Brudzinski, M. R., and Currie, B. S. Distinguishing induced seismicity from natural seismicity in Ohio: Demonstrating the utility of waveform template matching. *Journal of Geophysical Research: Solid Earth*, 120(9):6284–6296, Sept. 2015. doi: 10.1002/2015jb012265.

Skoumal, R. J., Ries, R., Brudzinski, M. R., Barbour, A. J., and Currie, B. S. Earthquakes Induced by Hydraulic Fracturing Are Pervasive in Oklahoma. *Journal of Geophysical Research: Solid Earth*, 123 (12), Dec. 2018. doi: 10.1029/2018jb016790.

Skoumal, R. J., Brudzinski, M. R., Currie, B. S., and Ries, R. Temporal patterns of induced seismicity in Oklahoma revealed from multi-station template matching. *Journal of Seismology*, 24(5): 921–935, Aug. 2019. doi: 10.1007/s10950-019-09864-9.

Skoumal, R. J., Barbour, A. J., Brudzinski, M. R., Langenkamp, T., and Kaven, J. O. Induced Seismicity in the Delaware Basin, Texas. *Journal of Geophysical Research: Solid Earth*, 125(1), Jan. 2020. doi: 10.1029/2019jb018558.

Steeples, D. W., Bennett, B. C., Park, C. B., Miller, R. D., and Knapp,

R. W. Microearthquakes in Kansas and Nebraska, 1977-1989; final report for contract NRC-04-87-084 to U.S. Nuclear Regulatory Commission. *Kansas Geological Survey, Open-file Report*, 90-10(4), Oct. 1990. http://www.kgs.ku.edu/Geophysics/OFR/1990/OFR90_10/index.html.

van der Elst, N. J. B-Positive: A Robust Estimator of Aftershock Magnitude Distribution in Transiently Incomplete Catalogs. *Journal of Geophysical Research: Solid Earth*, 126(2), Feb. 2021. doi: 10.1029/2020jb021027.

Verdecchia, A., Cochran, E. S., and Harrington, R. M. Fluid-Earthquake and Earthquake-Earthquake Interactions in Southern Kansas, USA. *Journal of Geophysical Research: Solid Earth*, 126(3), Mar. 2021. doi: 10.1029/2020jb020384.

Vidale, J. E. and Shearer, P. M. A survey of 71 earthquake bursts across southern California: Exploring the role of pore fluid pressure fluctuations and aseismic slip as drivers. *Journal of Geophysical Research: Solid Earth*, 111(B5), May 2006. doi: 10.1029/2005jb004034.

Wiemer, S. Minimum Magnitude of Completeness in Earthquake Catalogs: Examples from Alaska, the Western United States, and Japan. *Bulletin of the Seismological Society of America*, 90(4): 859–869, Aug. 2000. doi: 10.1785/0119990114.

Yeck, W. L., Weingarten, M., Benz, H. M., McNamara, D. E., Bergman, E. A., Herrmann, R. B., Rubinstein, J. L., and Earle, P. S. Far-field pressurization likely caused one of the largest injection induced earthquakes by reactivating a large preexisting basement fault structure. *Geophysical Research Letters*, 43(19), Oct. 2016. doi: 10.1002/2016gl070861.

Yeck, W. L., Hayes, G. P., McNamara, D. E., Rubinstein, J. L., Barnhart, W. D., Earle, P. S., and Benz, H. M. Oklahoma experiences largest earthquake during ongoing regional wastewater injection hazard mitigation efforts. *Geophysical Research Letters*, 44 (2):711–717, Jan. 2017. doi: 10.1002/2016gl071685.

Zhai, G., Shirzaei, M., Manga, M., and Chen, X. Pore-pressure diffusion, enhanced by poroelastic stresses, controls induced seismicity in Oklahoma. *Proceedings of the National Academy of Sciences*, 116(33):16228–16233, July 2019. doi: 10.1073/pnas.1819225116.

Zhai, G., Shirzaei, M., and Manga, M. Elevated Seismic Hazard in Kansas Due to High-Volume Injections in Oklahoma. *Geophysical Research Letters*, 47(5), Mar. 2020. doi: 10.1029/2019gl085705.